RESEARCH ARTICLE

ADVANCED
ENERGY & SUSTAINABILITY
RESEARCH
Open Access

www.advenergysustres.com

Comparative Analysis of Aqueous and Nonaqueous Polymer Binders for the Silicon Anode in All-Solid-State Batteries

Siyu An, Yuan Ma,* Seyedhosein Payandeh,* Andrey Mazilkin, Ruizhuo Zhang, Jürgen Janek, Aleksandr Kondrakov, and Torsten Brezesinski*

Silicon (Si) is anticipated to become one of the most promising anode materials for high-energy-density solid-state battery (SSB) applications owing to its high theoretical specific capacity and low working potential. This work compares the electrochemical behavior of slurry-cast electrodes in Si|Li$_6$PS$_5$Cl|In/InLi cells, with micron-sized Si particles ($\geq$99% active electrode material content) and polyacrylic acid (PAA) or polyvinylidene fluoride (PVDF) serving as active material and aqueous/nonaqueous model binder, respectively. The cycling stability of Si-PVDF cells is found to decrease with increasing binder content (accelerated capacity fade), whereas the Si-PAA cells show more or less the opposite trend. However, they exhibit a similar performance when using 0.5 wt% binder, with specific capacities of $\approx$850 mAh g^{-1} (for $-$0.51–0.11 V vs In/InLi) and high capacity retention depending on the cutoff potentials. This result suggests that PVDF can be substituted for by PAA in Si anodes for SSBs, thereby potentially decreasing cost and environmental impact.

1. Introduction

Solid-state Li-ion batteries (LIBs) are regarded as one of the most promising energy-storage technologies of the future.[1,2] The use of inorganic solid electrolytes (SEs) can enhance safety by replacing the flammable liquid electrolyte employed in conventional secondary batteries.[2–6] In addition, inorganic SEs have a high Li$^+$ transference number ($t_{Li+} \gg 0.5$) and may exhibit favorable mechanical properties. Hence, they are believed to enable stable cycling of high-capacity alloying and/or lithium-metal anodes, which are known to suffer from large volume variations during cycling, ultimately leading to improvements in cell-level energy density.[1,7,8] Thanks to the successful development of highly ionically conductive sulfide (thiophosphate) SEs such as argyrodite Li$_6$PS$_5$Cl (referred to as LPSCl hereafter; with $\sigma_{ion} \approx 2$ mS cm^{-1} at room temperature), solid-state batteries (SSBs) are also capable, in principle, of fast charging.[2,9,10]

Apart from the superionic SE, both anode and cathode materials are a central component of SSBs, determining the energy density, energy efficiency, and cycle life, among others.[11,12] A variety of anode materials have been developed and primarily tested in conventional LIB environments, encompassing intercalation- and insertion-type anodes such as graphite and Li$_4$Ti$_5$O$_{12}$, respectively, as well as alloying and conversion anodes.[13,14] Among them, the lithium-metal anode exhibits

S. An, Y. Ma,[+] S. Payandeh, A. Mazilkin, R. Zhang, J. Janek, A. Kondrakov, T. Brezesinski
Institute of Nanotechnology
Battery and Electrochemistry Laboratory (BELLA)
Karlsruhe Institute of Technology (KIT)
Hermann-von-Helmholtz-Platz 1, 76344 Eggenstein-Leopoldshafen, Germany
E-mail: yuan.ma@seu.edu.cn; a.payande88@gmail.com; torsten.brezesinski@kit.edu

The ORCID identification number(s) for the author(s) of this article can be found under https://doi.org/10.1002/aesr.202300092.

[+]Present address: Key Laboratory of Energy Thermal Conversion and Control of Ministry of Education, School of Energy and Environment, Southeast University, Nanjing 211189, Jiangsu, China

J. Janek
Institute of Physical Chemistry & Center for Materials Research (ZfM/LaMa)
Justus-Liebig-University Giessen
Heinrich-Buff-Ring 17, 35392 Giessen, Germany

A. Kondrakov
BASF SE
Carl-Bosch-Strasse 38, 67056 Ludwigshafen, Germany

some very exciting properties, including high theoretical specific capacity ($\approx$3860 mAh g^{-1}) and low working (redox) potential (-3.04 V vs standard hydrogen electrode). However, its large-scale industrial application in LIBs and SSBs remains constrained by various factors (interface instability, tendency for dendrite formation, etc.).[12,15]

Silicon is capable of delivering a similar specific capacity (e.g., 3579 mAh g^{-1} for Li$_{15}$Si$_4$) and is further abundant (inexpensive), environmentally friendly, and easier to handle and process, making it promising for use as an alloying-type negative electrode material not only in liquid electrolyte-based batteries but also in SSBs.[16,17] Kim et al. investigated the cycling performance of LPSCl-infiltrated, tape-cast anodes using micron-sized and nanoscale Si and incorporating polyvinylidene fluoride (PVDF) or cross-linked polyacrylic acid (PAA)/sodium carboxymethyl cellulose (CMC) as polymer binder.[18] Some encouraging results were obtained for the nano-Si electrode with PVDF (10 wt%). Tan et al. recently reported on a quasipure microsilicon anode (99.9 wt%) system that is free of carbon additives and SE but contains 0.1 wt% PVDF. The assembled SSB full cell, Si|Li$_6$PS$_5$Cl|NCM811 (NCM811 refers to LiNi$_x$Co$_y$Mn$_z$O$_2$ with 80% Ni content), delivered a specific discharge capacity of 1100 mAh g^{-1} and achieved a capacity retention of $\approx$80% after 500 cycles.[19] This result indicates that PVDF holds promise for application in Si-based SSB anodes. However, despite the apparent advantages, the development of Si electrodes for solid-state energy-storage applications is still in its infancy.[12] Apart from that, the processing of PVDF requires N-methyl-2-pyrrolidone (NMP), which itself is toxic, as organic solvent. Furthermore, spent NMP is difficult to recycle, thus calling for investigations into aqueous electrode processing routes with more sustainable ("green") polymer binders.

In the present work, we examine the effect that both polymer binder type and content ($\leq$1 wt%) have on the cyclability of tape-cast electrodes with micron-sized Si particles ($\geq$99 wt%) and the possibility of using a water-soluble binder in the manufacturing process (PAA vs PVDF). The electrochemical behavior of the µSi electrodes was investigated in half-cells with LPSCl and In/InLi as SE separator and counter electrode, respectively. Conducting research on Si-PVDF and Si-PAA is intended to provide a more comprehensive understanding of how different binder systems affect the cycling performance and stability of high-content Si electrodes, and this appears to be crucial for developing high-capacity SSB anodes. It should be noted though that PVDF and PAA served as model binders, and the conclusions drawn are specific to the context of this study. Nevertheless, the findings provide new insights, and they contribute to set a foundation for future research in the field.

2. Results and Discussion

Figure 1a schematically illustrates the structure and composition of the slurry-cast electrode as well as the configuration of the
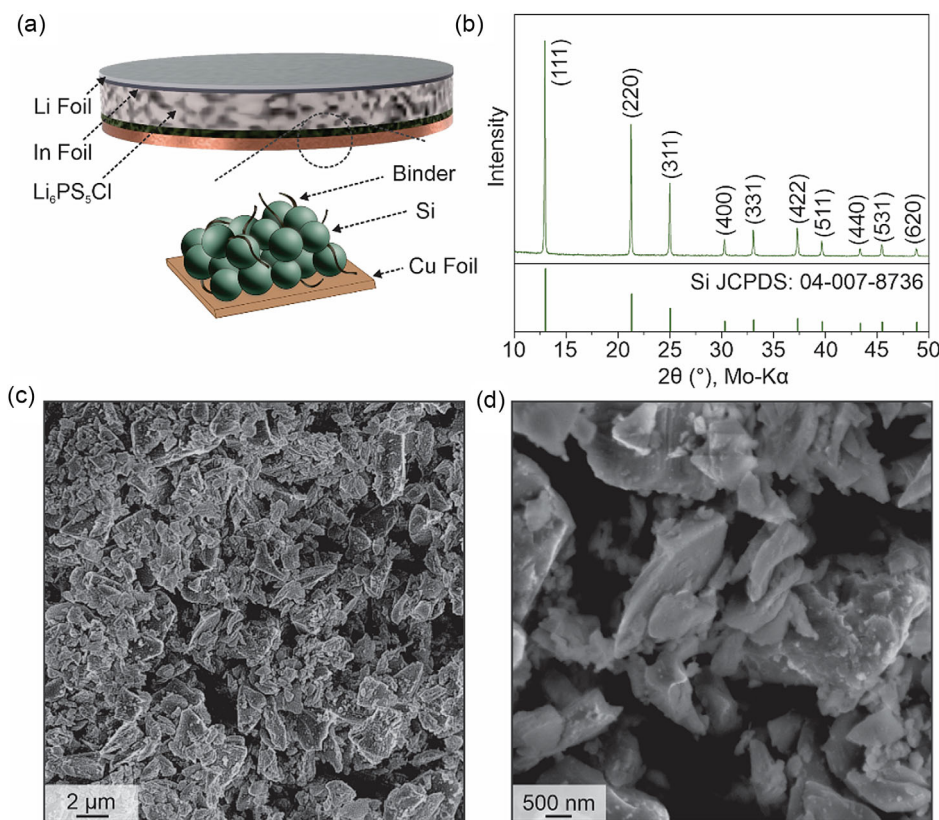

Figure 1. a) Schematic depiction of the Si|Li$_6$PS$_5$Cl|In/InLi SSB cell with slurry-cast µSi electrode. b) XRD pattern collected from the pristine µSi material and c,d) corresponding SEM images at different magnifications.

Si|Li$_6$PS$_5$Cl|In/InLi cell. The individual steps of the fabrication process are described in the Experimental Section. The structural/morphological characterization results for the pristine μSi material employed here are summarized in Figure 1b–d. The X-ray diffraction (XRD) pattern in Figure 1b shows reflections that can be indexed to the cubic phase of Si ($Fd-3m$ space group), with no signs of crystalline impurities. The scanning electron microscopy (SEM) images in Figure 1c,d indicate that the particles are agglomerated to some degree and have a nonuniform morphology (exhibiting a variety of shapes). The particle size ranges from ≈1 to 5 μm.

Specifically, high-content μSi electrodes with 0.1, 0.5, and 1.0 wt% PVDF or PAA binder were studied in this work (more details on the composition are given in Table S1, Supporting Information). Representative cross-sectional high-angle annular dark-field (HAADF) scanning transmission electron microscopy (STEM) images of the Si-PVDF and Si-PAA electrodes with a binder content of 0.5 wt% (referred to as Si-PVDF-0.5 and Si-PAA-0.5 hereafter) in pristine state, i.e., prior to cycling, are shown in **Figure 2**a,d. As is evident, they have comparable structures on the micrometer level with a similar degree of residual porosity. Regardless of the different processing, aqueous versus nonaqueous, the surface of the μSi particles was found to be covered by a ≈1 nm-thick shell of SiO$_x$ in both cases (see results from TEM and energy-dispersive X-ray spectroscopy [EDS] mapping in Figure 2b,c,e,f; note that unlike PVDF, PAA is contributing to the oxygen signal detected by EDS). The presence of a native oxide layer is believed to be due to exposure to the external atmosphere rather than an issue of the solvents.

The cyclability of the slurry-cast μSi electrodes in Si|Li$_6$PS$_5$Cl|In/InLi cells was examined first in the potential range between −0.57 and 0.38 V versus In/InLi (≈0.05–1.0 V vs Li$^+$/Li) at 45 °C. μSi has been shown to exhibit an electronic conductivity of ≈10^{-5} S cm^{-1} at room temperature, similar to that of layered
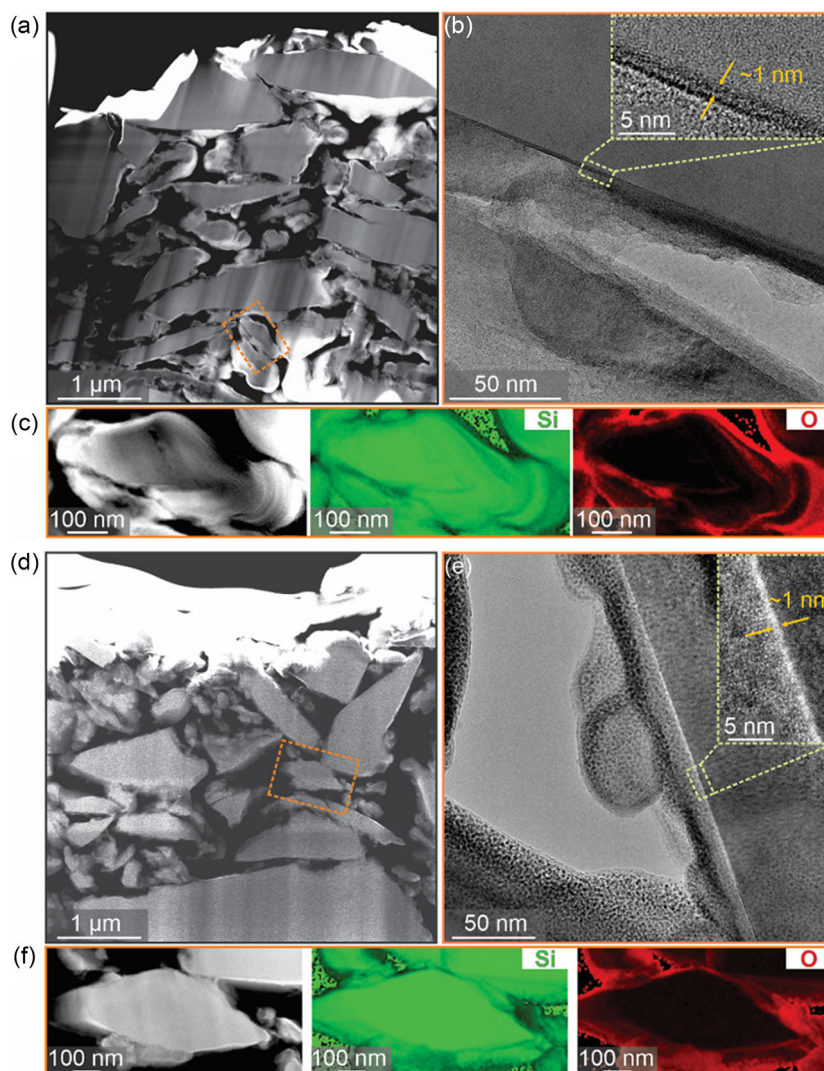

Figure 2. Electron microscopy of the as-prepared a–c) Si-PVDF-0.5 and d–f) Si-PAA-0.5 electrodes. a,d) Cross-sectional HAADF STEM images. b,e) Magnified images of the μSi particle surface. The insets reveal the presence of a thin SiO$_x$ shell. c,f) EDS mapping of the region denoted by the orange box in a) and d).

**ADVANCED
SCIENCE NEWS**

www.advancedsciencenews.com

**ADVANCED
ENERGY & SUSTAINABILITY
RESEARCH**
Open Access

www.advenergysustres.com

oxide cathode materials (note that for the latter the bulk electronic conductivity typically increases by orders of magnitude with delithiation during charge) such as $LiCoO_2$ (LCO) and NCM (or NMC), thus the use of carbon black/graphite in the electrode is not imperative.[19–22]

Figure 3a–d shows the Coulomb efficiencies and specific delithiation capacities (corresponding to the discharge process in full cells) over the first 52 cycles. In the initial cycles, the C-rate was gradually increased from 0.05 to 0.2C. For the PVDF-containing cells, the first-cycle capacity decreased with increasing binder content, from $3032\,mAh\,g^{-1}$ for Si-PVDF-0.1 to $2300\,mAh\,g^{-1}$ for Si-PVDF-1.0 (see voltage profiles of the first two cycles in Figure S1a–c, Supporting Information). The variation in delithiation capacity was somewhat less pronounced among the Si-PAA electrodes (see Figure S2a–c, Supporting Information), with Si-PAA-0.5 delivering the highest specific capacity at 0.05C ($q_{dis} = 3111\,mAh\,g^{-1}$ in the initial cycle). The second-cycle differential capacity (dq/dV) curves shown in Figures S1d and S2d (Supporting Information) demonstrate that all electrodes underwent basically the same de-/lithiation processes, in line with expectations. Regarding the Coulomb efficiency (see also Table S2 and S3, Supporting Information), the Si-PAA electrodes revealed a slightly better reversibility in the initial cycle than the Si-PVDF ones, with, e.g., 84.2% for Si-PVDF-0.5 and 85.1% for Si-PAA-0.5. In general, the reversibility increased with cycling, independent of the binder type and content. The average Coulomb efficiency between cycle 10 and 52 stabilized at ≈99% for all cells tested. Unlike Si-PAA cells, the Si-PVDF cells showed accelerated capacity loss at 0.2C cycling with increasing binder content. The capacity retention after 52 cycles relative to the fifth cycle varied from 37% for Si-PVDF-0.1 to 31% for Si-PVDF-1.0, compared to 36% for Si-PAA-0.1% and 50% for Si-PAA-1.0 (see Table S2 and S3, Supporting Information). A possible explanation for this might be improved bonding between PAA and SiO_x and/or Si (i.e., robust [supramolecular] interfacial interactions, as opposed to weak van der Waals interactions in the case of PVDF), which helps better accommodate the volume variation of the μSi particles upon de-/alloying with lithium during battery operation.[23–25] Another explanation might be that the larger relative volume fraction of PAA (higher degree of particle coverage, due to lower density) is one of the factors contributing to the better performance (improved electrode integrity). Unfortunately, the preparation and/or testing of electrodes with a higher binder content (5 wt%) failed. However, differences in electron transfer across the binder-coated particles cannot be ruled out. It should be noted that, in general, increasing the binder content impairs both ionic and electronic charge transport through the electrode, ultimately resulting in impedance buildup (see dq/dV curves in Figure S1d, Supporting Information, for example) and capacity degradation. For that reason and because some of the cycling performance metrics were similar for Si-PVDF-0.5 and Si-PAA-0.5, the latter electrodes were studied in more detail during the course of this work.

For improving the stability (capacity retention), the slurry-cast μSi electrodes were cycled in narrower potential windows of −0.50–0.10, −0.51–0.11, and −0.52–0.12 V versus In/InLi. The higher lithiation cutoff potentials correspond to ≈0.12, 0.11, and 0.10 V versus Li^+/Li, respectively, and were meant to limit the amorphization of the initially crystalline μSi material and partially prevent the formation of highly lithiated phases such as $Li_{3.5}Si$ (shallow cycling), thereby reducing the volume expansion/contraction during cycling.[26–28] Likewise, the delithiation cutoff potential has been shown to affect the longevity.

As can be seen from the voltage profiles at 0.05C rate in **Figure 4**a,c, the specific capacities achieved were lower with cycling in a narrower potential window, from $q_{dis} = 2881\,mAh\,g^{-1}$ in the initial cycle for −0.57 to 0.38 V (see Figures 3b and S1b, Supporting Information) to $708\,mAh\,g^{-1}$ for −0.50 to 0.10 V in the case of Si-PVDF-0.5 ($1047\,mAh\,g^{-1}$ for −0.51 to 0.11 V, $1589\,mAh\,g^{-1}$ for −0.52 to 0.12 V) and from $q_{dis} = 3111\,mAh\,g^{-1}$ for −0.57 to 0.38 V (see Figure 3d and S2b, Supporting Information) to $653\,mAh\,g^{-1}$ for −0.50 to 0.10 V for Si-PAA-0.5 ($1215\,mAh\,g^{-1}$ for −0.51 to 0.11 V, $2153\,mAh\,g^{-1}$ for −0.52 to
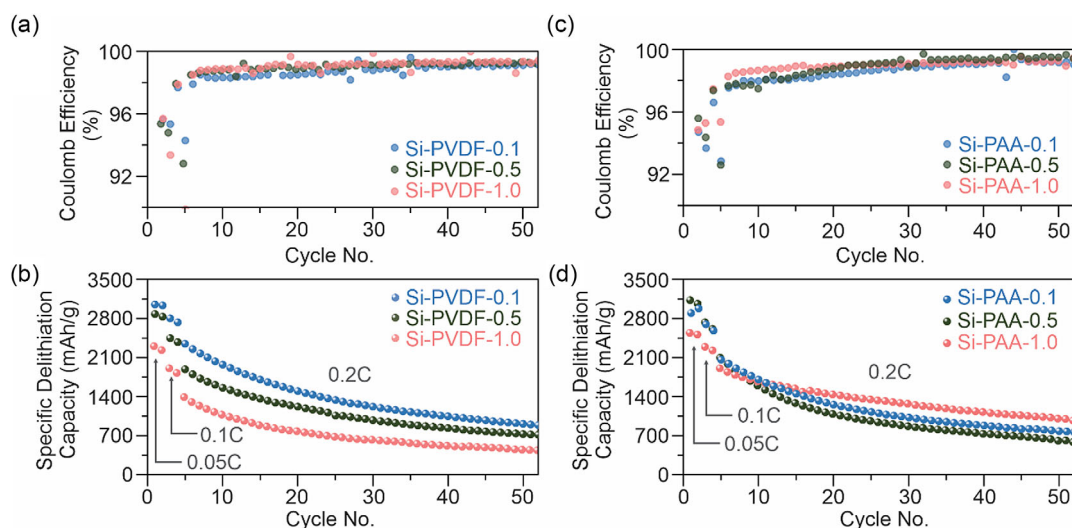

Figure 3. a,c) Coulomb efficiency and b,d) cycling stability of the Si-PVDF and Si-PAA electrodes in Si|Li$_6$PS$_5$Cl|In/InLi SSB cells in the potential window of −0.57 to 0.38 V versus In/InLi at 45 °C.
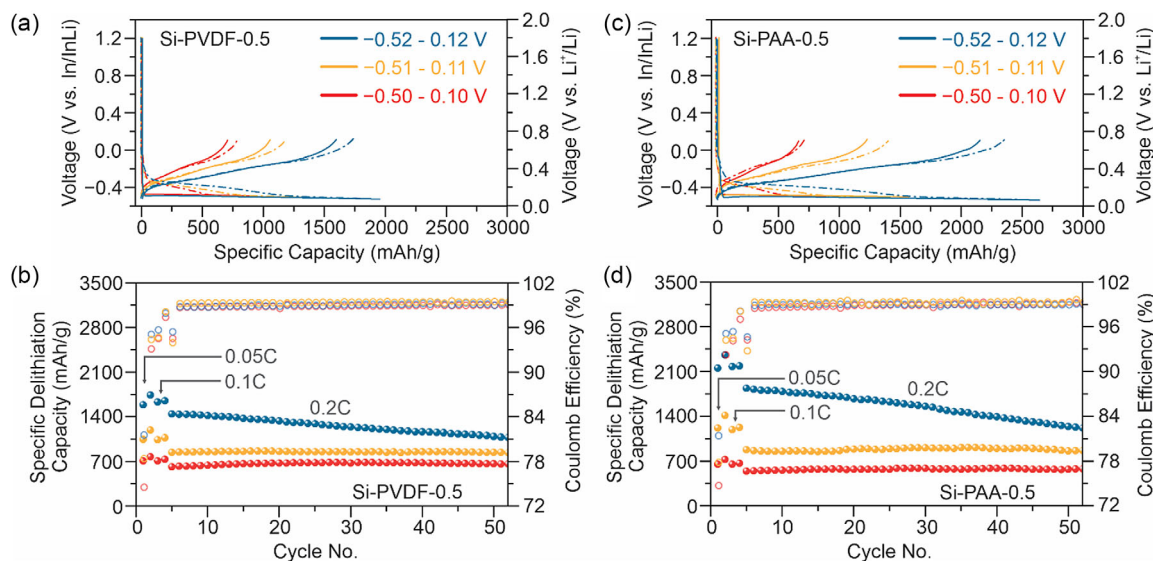
Figure 4. Cyclability of the Si-PVDF-0.5 and Si-PAA-0.5 electrodes in Si|Li$_6$PS$_5$Cl|In/InLi SSB cells in the potential windows of −0.50 to 0.10 V, −0.51 to 0.11 V, and −0.52 to 0.12 V versus In/InLi at 45 °C. a,c) First- (solid line) and second-cycle (dashed line) voltage profiles at 0.05C rate. b,d) Coulomb efficiency (open symbols) and specific delithiation capacity (solid symbols) plotted against the cycle number.

0.12 V). Although the degree of lithiation decreased with increasing lower cutoff potential, all electrodes underwent the same phase transition (see Figure S3, Supporting Information), but to different extents.[27] Despite sacrificing capacity, the cycling stability was much improved, especially for the potential windows of −0.50 to 0.10 V and −0.51 to 0.11 V, with virtually 100% capacity retention after 52 cycles relative to the fifth cycle at 0.2C (see Figure 4b,d as well as Table S4 and S5, Supporting Information; voltage profiles for the cycles 10–50 are presented in Figure S4 and S5, Supporting Information), compared to only 27–38% for the same electrodes cycled between −0.57 and 0.38 V (see Figure 3b,d as well as Table S2 and S3, Supporting Information). This result demonstrates that the cutoff potentials play an important role and must be tailored for maximum performance and stability (in addition to the properties of the active material). The average Coulomb efficiency was highest for −0.51 to 0.11 V and reached 99.5% for both the Si-PVDF-0.5 and Si-PAA-0.5 cells (see also Table S4 and S5, Supporting Information). No apparent differences between the Si-PVDF-0.5 and Si-PAA-0.5 were observed in this series of electrochemical experiments, thus indicating that PVDF can be substituted for by an aqueous binder (PAA) in Si anodes for SSB applications.

Although the present study cannot be directly compared with that reported by Tan et al.,[19] due to differences in the experimental conditions and testing parameters (counter electrode, cell assembly, external pressure applied during operation etc.), this work achieved a promising result, demonstrating enhanced stability by restricting the capacity utilization. Overall, it seems likely that the Si-PVDF-0.5 and Si-PAA-0.5 cells are capable of maintaining good capacity retention during long-term cycling and in different cell configurations, yet this needs further study.

Finally, postmortem SEM measurements were conducted on the slurry-cast μSi electrodes to gain some insight into their structure/morphology evolution upon cycling. **Figure 5**a–i shows

cross-sectional and top-view images along with elemental mapping results for the Si-PVDF-0.5 and Si-PAA-0.5 electrodes before and after cycling in the potential range between −0.51 and 0.11 V versus In/InLi (imaging and mapping data for the other potential windows applied are shown in Figure S6–S10, Supporting Information). From the cross-sectional SEM and EDS results, it is apparent that both the Si-PVDF-0.5 and Si-PAA-0.5 underwent an irreversible volume expansion of more than 100% and a major fraction of the residual porosity—pore space between the μSi particles—vanished after cycling for 52 cycles (see Figure 2a,d for comparison). As expected, the increase in electrode thickness varied with the cutoff potential (decreasing with narrowing potential window). The same holds true for the degree of cracking/electrode fracture. Notably, top-view SEM imaging revealed moderate cracking for cycling between −0.51 and 0.11 V. These findings agree well with the trends observed from electrochemical testing and further emphasize the similarity between the Si-PVDF-0.5 and Si-PAA-0.5 cells.

In recent years, the chemical and electrochemical decomposition of thiophosphate SEs has been widely investigated,[2,10,29–32] and for conventional LIBs, different binders have been shown to lead to different degrees of interphase formation.[33] Here, the Si-PVDF-0.5 and Si-PAA-0.5 electrodes were eventually cycled in a relatively narrow potential window and found to exhibit similar performance and stability. This is corroborated by electrochemical impedance spectroscopy (EIS) data collected from the cells after cycling, indicating that the type of binder has no notable effect on the cell resistance (for low binder content scenarios; see Nyquist plots of the electrochemical impedance in Figure S11, Supporting Information). Ex situ SEM analysis also revealed comparable levels of cracking in both electrodes. From these results, it can be concluded that 1) there are no major differences in Si|LPSCl interface degradation and 2) both PAA and PVDF exert a similar effect on the slurry-cast μSi electrode, when
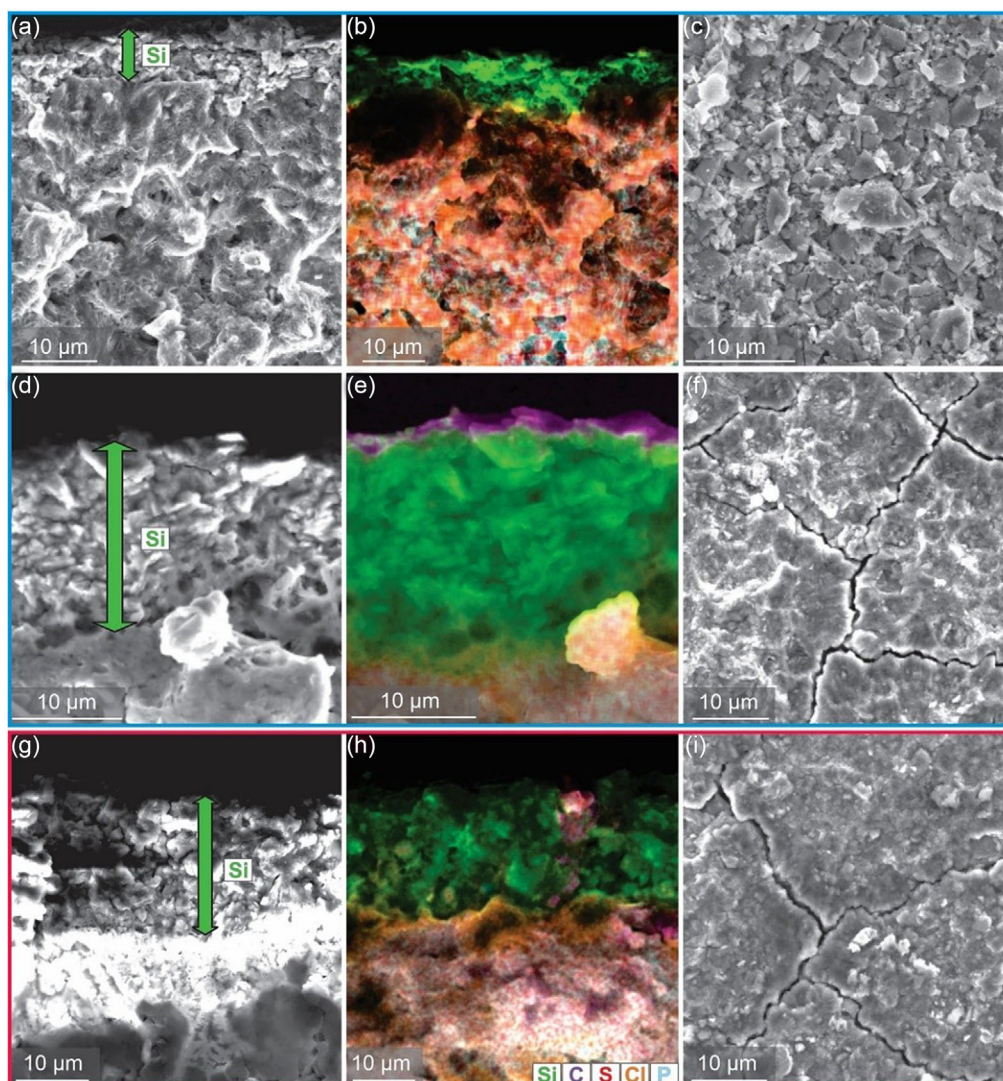
**ADVANCED
SCIENCE NEWS**

www.advancedsciencenews.com

**ADVANCED
ENERGY & SUSTAINABILITY
RESEARCH**
Open Access

www.advenergysustres.com

Figure 5. a,d,g) Cross-sectional SEM images, b,e,h) corresponding EDS mapping results, and c,f,i) top-view SEM images of a–f) the Si-PVDF-0.5 and g–i) Si-PAA-0.5 electrodes. Data acquired a–c) before cycling and d–i) after 52 cycles at 45 °C in the potential window of −0.51 to 0.11 V versus In/InLi.

the binder content is low. This highlights the promise of aqueous electrode processing routes with more sustainable binders.

3. Conclusions

In summary, carbon-free, high-content μSi electrodes were successfully produced by slurry casting using PAA and PVDF as model binders. The effect that aqueous and nonaqueous processing conditions have on the performance of Si|Li$_6$PS$_5$Cl|In/InLi solid-state battery cells was investigated. In contrast to PAA, PVDF-containing electrodes showed accelerated capacity degradation with increasing binder content. Tape-cast μSi electrodes with 0.5 wt% PAA or PVDF binder were studied in some more detail and found to exhibit similar performance. They were capable of delivering reversible specific capacities of ≈850 mAh g^{-1} at 0.2C rate and 45 °C upon cycling in a potential window of −0.51 to 0.11 V versus In/InLi and showed favorable mechanical

behavior (presence of few cracks on the micrometer length scale), despite a relatively large irreversible volume change during battery operation. Overall, our research data indicate that PVDF can be substituted for by a functional, aqueous binder (PAA) toward the realization of sustainable and environmentally friendly Si anodes for solid-state battery applications. This provides a new perspective for future research. However, whether other "green" polymer binders such as CMC or poly(vinyl alcohol) (PVA) can be used as viable alternatives to PVDF requires further study.

4. Experimental Section

Preparation of Slurry-Cast Si Electrodes: Micron-sized Si (Thermo Fisher Scientific) and PAA (25 wt% solution in water, M.W. 240000; Acros Organics) or PVDF (Solef 5130; Solvay GmbH) polymer binder were used in the electrode manufacturing. First, 1 wt% aqueous PAA and 0.5 wt% NMP-based PVDF solutions were prepared. Then, Si powder and binder

solution were combined, aiming at the compositions given in Table S1 (Supporting Information), followed by mixing at 2000 rpm for 15 min. The solid content of the slurries was in the range of 50%. They were cast onto Cu foil (80 μm wet-film thickness) with the help of an electromotive film applicator (COATMASTER 510; ERICHSEN GmbH & Co. KG). The resulting electrodes were placed in a vacuum oven (VDL 53; Binder GmbH) and dried at 80 °C in a dynamic vacuum for 12 h. The Si loading was ≈2 mg cm^{-2}.

Cell Assembly and Testing: A customized cell setup with 10 mm inner diameter was used for SSB testing. It consisted of three major parts, namely, stainless steel current collectors at both ends and a ring made of PEEK in the middle, in which the pellet was pressed. The entire assembling process was carried out in an Ar glove box. About 100 mg LPSCl SE (NEI Corp.) was placed in the PEEK ring and compacted at 62 MPa for 3 min. Then, 9 mm diameter Si tape was placed on one end of the separator layer, and a pressure of 434 MPa was applied for 3 min. Next, 9 mm diameter In foil of thickness 127 μm (Sigma–Aldrich) and Li foil of thickness 50 μm (Albemarle Germany GmbH) were attached to the other side, and a pressure of 124 MPa was applied for 3 min. Finally, the cell was placed in a special pressure rig.

Galvanostatic charge/discharge measurements were performed at 45 °C and at different C-rates (with 1.0C = 3000 mA g^{-1}) while applying an external pressure of 81 MPa. Electrochemical testing of the SSB cells was primarily done in the potential range from −0.57 to 0.38 V versus In/InLi (equivalent to ≈0.05–1.0 V vs Li$^+$/Li) after a resting period at open-circuit voltage for 1 h using a MACCOR battery cycler. EIS measurements were conducted on the cells after cycling at 45 °C (10 mV voltage amplitude, 7 MHz to 4 mHz frequency change) using a SP-300 multichannel potentiostat (BioLogic).

Characterization: The surface morphology of pristine Si electrodes and cycled ones collected from disassembled SSB cells was investigated by SEM using a LEO-1530 microscope (Carl Zeiss AG) with a field emission source. Powder XRD data were collected on a STOE Stadi-P diffractometer with a DECTRIS MYTHEN 1 K strip detector. The instrument uses a Mo anode ($\lambda = 0.70926$ Å). The samples for XRD were flame-sealed in borosilicate capillaries of 0.68 mm inner diameter and 0.01 mm wall thickness (Hilgenberg). TEM was conducted on specimens at 300 kV using a double-corrected Themis-Z microscope (Thermo Fisher Scientific). Specimen cross sections were prepared by means of a dual-beam focused Ga-ion beam in an FEI Strata 400 at 30 kV, followed by cleaning at 5 and 2 kV.

Supporting Information

Supporting Information is available from the Wiley Online Library or from the author.

Acknowledgements

Conflict of Interest

The authors declare no conflict of interest.

Data Availability Statement

The data that support the findings of this study are available from the corresponding author upon reasonable request.

[1] J. Janek, W. G. Zeier, *Nat. Energy* **2016**, *1*, 16141.

[2] A. Banerjee, X. Wang, C. Fang, E. A. Wu, Y. S. Meng, *Chem. Rev.* **2020**, *120*, 6878.

[3] Y. Ma, R. Zhang, Y. Tang, Y. Ma, J. H. Teo, T. Diemant, D. Goonetilleke, J. Janek, M. Bianchini, A. Kondrakov, T. Brezesinski, *ACS Nano* **2022**, *16*, 18682.

[4] Y. Ma, J. H. Teo, D. Kitsche, T. Diemant, F. Strauss, Y. Ma, D. Goonetilleke, J. Janek, M. Bianchini, T. Brezesinski, *ACS Energy Lett.* **2021**, *6*, 3020.

[5] R. Chen, Q. Li, X. Yu, L. Chen, H. Li, *Chem. Rev.* **2020**, *120*, 6820.

[6] L. Zhou, C. Y. Kwok, A. Shyamsunder, Q. Zhang, X. Wu, L. F. Nazar, *Energy Environ. Sci.* **2020**, *13*, 2056.

[7] Y.-G. Lee, S. Fujiki, C. Jung, N. Suzuki, N. Yashiro, R. Omoda, D.-S. Ko, T. Shiratsuchi, T. Sugimoto, S. Ryu, J. H. Ku, T. Watanabe, Y. Park, Y. Aihara, D. Im, I. T. Han, *Nat. Energy* **2020**, *5*, 299.

[8] K. Xu, *Chem. Rev.* **2014**, *114*, 11503.

[9] K. H. Park, Q. Bai, D. H. Kim, D. Y. Oh, Y. Zhu, Y. Mo, Y. S. Jung, *Adv. Energy Mater.* **2018**, *8*, 1800035.

[10] Y. Ma, J. H. Teo, F. Walther, Y. Ma, R. Zhang, A. Mazilkin, Y. Tang, D. Goonetilleke, J. Janek, M. Bianchini, T. Brezesinski, *Adv. Funct. Mater.* **2022**, *32*, 2111829.

[11] N. Nitta, F. Wu, J. T. Lee, G. Yushin, *Mater. Today* **2015**, *18*, 252.

[12] H. Huo, J. Janek, *ACS Energy Lett.* **2022**, *7*, 4005.

[13] J. Lu, Z. Chen, F. Pan, Y. Cui, K. Amine, *Electrochem. Energy Rev.* **2018**, *1*, 35.

[14] P. Oh, J. Yun, J. H. Choi, K. S. Saqib, T. J. Embleton, S. Park, C. Lee, J. Ali, K. Ko, J. Cho, *Angew. Chem., Int. Ed.* **2022**, *61*, e202201249.

[15] T. Krauskopf, B. Mogwitz, H. Hartmann, D. K. Singh, W. G. Zeier, J. Janek, *Adv. Energy Mater.* **2020**, *10*, 2000945.

[16] G. Zhu, D. Chao, W. Xu, M. Wu, H. Zhang, *ACS Nano* **2021**, *15*, 15567.

[17] C. Zhang, F. Wang, J. Han, S. Bai, J. Tan, J. Liu, F. Li, *Small Struct.* **2021**, *2*, 2100009.

[18] D. H. Kim, H. A. Lee, Y. B. Song, J. W. Park, S.-M. Lee, Y. S. Jung, *J. Power Sources* **2019**, *426*, 143.

[19] D. H. S. Tan, Y.-T. Chen, H. Yang, W. Bao, B. Sreenarayanan, J.-M. Doux, W. Li, B. Lu, S.-Y. Ham, B. Sayahpour, J. Scharf, E. A. Wu, G. Deysher, H. E. Han, H. J. Hah, H. Jeong, J. B. Lee, Z. Chen, Y. S. Meng, *Science* **2021**, *373*, 1494.

[20] Z. Chen, C. Wang, J. Lopez, Z. Lu, Y. Cui, Z. Bao, *Adv. Energy Mater.* **2015**, *5*, 1401826.

[21] S. Burkhardt, M. S. Friedrich, J. K. Eckhardt, A. C. Wagner, N. Bohn, J. R. Binder, L. Chen, M. T. Elm, J. Janek, P. J. Klar, *ACS Energy Lett.* **2019**, *4*, 2117.

[22] X.-Y. Qiu, Q.-C. Zhuang, Q.-Q. Zhang, R. Cao, P.-Z. Ying, Y.-H. Qiang, S.-G. Sun, *Phys. Chem. Chem. Phys.* **2012**, *14*, 2617.

[23] A. Magasinski, B. Zdyrko, I. Kovalenko, B. Hertzberg, R. Burtovyy, C. F. Huebner, T. F. Fuller, I. Luzinov, G. Yushin, *ACS Appl. Mater. Interfaces* **2010**, *2*, 3004.

[24] W. Huang, W. Wang, Y. Wang, Q. Qu, C. Jin, H. Zheng, *J. Mater. Chem. A* **2021**, *9*, 1541.

[25] T.-W. Kwon, J. W. Choi, A. Coskun, *Joule* **2019**, *3*, 662.

**ADVANCED
SCIENCE NEWS**

www.advancedsciencenews.com

**ADVANCED
ENERGY & SUSTAINABILITY
RESEARCH**
Open Access

www.advenergysustres.com

[26] M. N. Obrovac, L. Christensen, *Electrochem. Solid-State Lett.* **2004**, *7*, A93.

[27] M. J. Loveridge, M. J. Lain, I. D. Johnson, A. Roberts, S. D. Beattie, R. Dashwood, J. A. Darr, R. Bhagat, *Sci. Rep.* **2016**, *6*, 37787.

[28] M. Graf, C. Berg, R. Bernhard, S. Haufe, J. Pfeiffer, H. A. Gasteiger, *J. Electrochem. Soc.* **2022**, *169*, 20536.

[29] M. B. Dixit, N. Singh, J. P. Horwath, P. D. Shevchenko, M. Jones, E. A. Stach, T. S. Arthur, K. B. Hatzell, *Matter* **2020**, *3*, 2138.

[30] Y. Zhu, X. He, Y. Mo, *ACS Appl. Mater. Interfaces* **2015**, *7*, 23685.

[31] J. Auvergniot, A. Cassel, D. Foix, V. Viallet, V. Seznec, R. Dedryvère, *Solid State Ion.* **2017**, *300*, 78.

[32] Y. Xiao, Y. Wang, S.-H. Bo, J. C. Kim, L. J. Miara, G. Ceder, *Nat. Rev. Mater.* **2020**, *5*, 105.

[33] P. Parikh, M. Sina, A. Banerjee, X. Wang, M. S. D'Souza, J.-M. Doux, E. A. Wu, O. Y. Trieu, Y. Gong, Q. Zhou, K. Snyder, Y. S. Meng, *Chem. Mater.* **2019**, *31*, 2535.